

# Shaft Encoder Characterization via Theoretical Model of Differentiator with Both Differential and Integral Nonlinearities

Richard C. Kavanagh, *Member, IEEE*

**Abstract**—A model of an incremental shaft encoder is developed to facilitate sensor characterization. The model is obtained through derivation of a new mathematical formula for the spectral characteristics of the error which accrues when a sampled, nominally constant-rate signal is uniformly quantized, having been subject to both differential and integral nonlinearities. The spectrum of the error in the rate estimate generated when a digital differentiator is applied to such a signal is shown to be of particular importance. Subsequent sensor characterization involves some basic signal processing of a set of sampled sensor outputs, obtained when the encoder rotates at an almost uniform rate, followed by a simple curve-fitting procedure using the formula for estimated rate error. Both computer-generated, finite-length data sets and experimental data derived from encoder-based shaft velocity measurements are utilized to verify the theoretical model. The methodology of the mathematical analysis is applicable to other digital sensors and to a more general class of systems, such as data converters, which involve the digital differentiation of quantized, noise-affected signals. The paper illustrates how the combined influence of quantization error and of additional sources of noise can be described in an analytical, but applicable, manner.

**Index Terms**—Differentiation, digital measurements, optical transducers, optical velocity measurement, quantization, tachometers.

## NOMENCLATURE

$A$	Peak magnitude of sinusoidal perturbation.
$e$	Quantization noise (total error) of signal.
$e'$	Quantization error (e.g. of process $\{y\}$ ).
$f$	Frequency (per sample time).
$IS_e(f)$	Integrated spectrum of error signal
$IS_v(f)$	Integrated spectrum of rate error.
$J_m(\cdot)$	Bessel function of the $m$ th kind.
$k$	Index of discrete spectral component.
$k_{\max}$	Absolute maximum value of $k$ used in plot.
$L$	Number of encoder lines per revolution.
$m$	Index of sideband introduced by sinusoidal perturbation.
$N_i$	Length of finite data set.
$p, p_i$	Signal level (position); ditto at sample $i$ .
$P_e(f)$	Discrete spectral components of $e$ .
$P_{e'}(f)$	Discrete spectral components of $e'$ .
$P_v(f)$	Rate error spectrum of $e$ .
$P_{v'}(f)$	Rate error spectrum of $e'$ .

$q(\cdot)$	Function governing uniform quantizer.
$S_e(f)$	Power spectral density of signal error.
$S_v(f)$	Power spectral density of rate error.
$v_a$	Average rate of change of signal $p$ .
$\hat{v}$	Differentiator output (velocity estimate).
$w$	Noise process, usually uniformly distributed transition noise.
$w_s$	Noise (error) due to sinusoidal perturbation.
$y$	Input signal to ideal quantizer.
$\mathbb{Z}$	The set of integers.
$\varepsilon$	Magnitude of uniformly distributed noise (i.e. distributed over $[-\varepsilon, \varepsilon]$ ), relative to nominal position change of one bit.

## I. INTRODUCTION

THE output waveforms from incremental encoders are affected by a wide range of manufacturing nonidealities [1]. For the purpose of sensor characterization, it is clear from an evaluation of these nonidealities that the most significant error sources can be classified as differential or integral in nature.

New formulae were established in [2] for the rms and spectral errors associated with the digital differentiation of a uniformly quantized constant-rate signal which is affected by a uniformly distributed noise source. These formulae facilitated the development of a model of an optical shaft encoder with differential nonideality. The assumption of a constant rate signal with a uniformly distributed noise component was shown to reflect accurately the influence of this nonideality on the incremental-encoder-based velocity estimation of a rotating mass, at close to constant velocity. The primary thrust of this work is to develop a more comprehensive model which also accounts for integral nonlinearities.

Two distinct low-frequency effects applicable to incremental encoders can modify the error measures and spectra associated with the quantizer output error:

- 1) The actual angular velocity of the measurand will always exhibit some variation, due to inertial imbalance, bearing nonideality, influence of torque transmission compliance, motor controller limitations, etc.
- 2) An integral nonlinearity may be present in the encoder itself, whereby the bin transition locations exhibit a low-frequency variation from their ideal angular positions over the circumference of the encoder disk.

Both effects can be modeled by postulating the existence of an ideal quantizer with a perturbation of the input signal about its

Manuscript received April 1, 1999; revised January 20, 2000.

The author is with the Department of Electrical and Electronic Engineering, University College Cork, Cork, Ireland.

Publisher Item Identifier S 0018-9456(00)04814-2.

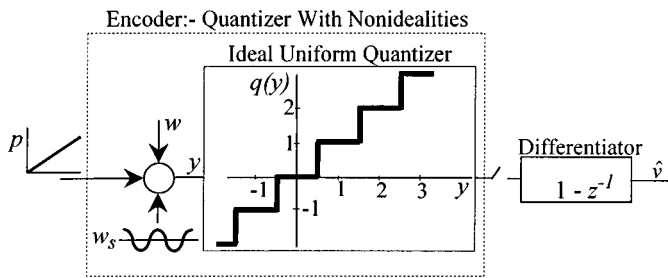


Fig. 1. Model of an optical shaft encoder, where the quantizer exhibits both a sinusoidal nonideality and uniformly distributed transition noise. A digital differentiator provides estimation of input rate.

previously assumed, constant rate characteristic. To a first-order approximation, this integral error can be represented by its first harmonic, a sinusoidal variation at a frequency corresponding to the angular rotational frequency of the encoder wheel (equal to that of the rotating inertia when a nongearing sensor is employed). This assumption is justified by the experimental observations of Yien [1], and verified by the excellent agreement between experimental and theoretical spectral characteristics obtained. In this paper, it will be assumed that the apparent sinusoidal variation is caused by sensor nonideality, rather than by shaft velocity variation, except where otherwise stated. Due to the similarity of the nature of the error spectra obtained in both cases, this assumption will be reasonable only when the mechanical set-up of the test structure is such as to minimize the first effect. Additionally, by characterizing the sensor over a wide range of angular velocities, the impact of the presence of velocity variation becomes evident, as discussed in Section IV.

The full encoder model, which also includes differential nonlinearity, modeled by a uniform noise source  $w$ , as well as the sinusoidal variation  $w_s$ , is shown in Fig. 1. Determination of sensor parameters reflecting the nonlinearities requires derivation of a formula for the spectrum of the rate error process defined by the difference between the actual shaft velocity and the velocity determined by the encoder/differentiator combination illustrated in Fig. 1.

The influence of a sinusoidal perturbation on the rate estimation can be derived in a manner analogous to that used in [3], [4] (and elsewhere) to analyze the quantization error which accrues when a purely sinusoidal signal is applied to a pulse-code modulator or sigma-delta converter. The application of the characteristic function approach to the analysis of almost periodic systems was extended to position sensors in [2]. An insight can also be obtained into the spectral consequences of the perturbation by comparison with some of the modulating schemes commonly adopted in communications systems. It is shown below that the spectrum of the sinusoidally perturbed, quantized signal is similar to that of a conventional, frequency modulated (FM), communications system, insofar as the generation of the resultant line intensities involves similar Bessel functions to those encountered in the textbook analysis of the sinusoidal modulation of a sinusoidal carrier [5], [6]. The principal distinction with frequency-modulated communications systems is that the sinusoidal carrier is replaced in this work by an almost periodic, quantization error signal. The spectra are found to possess similarities to those associated with pulse-width-modulated systems

[5], [7], the spectral components of the carrier having different modulating indices, some exhibiting a narrow-band characteristic while others are wide-band.

## II. MODEL OF SYSTEM WITH SINUSOIDAL PERTURBATION

Initially, the differential noise (termed transition noise in [2]) is ignored, so that the signal input to the ideal quantizer can be represented by a constant rate signal with an added sinusoidal perturbation

$$y_i = v_a i + A \sin(2\pi(v_a/L)i + \phi) \quad (1)$$

where  $v_a$  is the average rate,  $\phi$  is the phase of the sinusoidal contribution relative to the chosen origin, and  $L$  is the number of encoder lines per revolution. The sample index is represented by  $i$ . This formula is valid under the assumption that units of bits and bits per sample-time are used for the discrete samples of the signal and its rate, respectively. Recognizing that the error measures and spectra are independent of the choice of origin, being evaluated over an infinite domain,  $\phi$  can be set to zero without loss of generality.

As shown in Fig. 1, the noise-affected signal is assumed to be operated on by a regular quantizer, defined as in [2]

$$\begin{aligned} q(y) &= \lfloor y + \frac{1}{2} \rfloor = y + \frac{1}{2} - \langle y + \frac{1}{2} \rangle \\ e'(y) &= \langle y + \frac{1}{2} \rangle - \frac{1}{2} \end{aligned} \quad (2)$$

where  $e'(y)$  represents the quantization error of signal  $y$ , and  $\langle x \rangle$  and  $\lfloor x \rfloor$  represent the fractional part of  $x$  and the largest integer less than or equal to  $x$ , respectively. The Fourier series expansion of the error  $e'$ , [2], which yields

$$e'_i = \sum_{k \neq 0} -\frac{1}{2\pi jk} e^{2\pi jk y_i} \quad (3)$$

is useful in the analysis of the quantized system, as illustrated below. Regular samples of the quantizer output generate a quantization error process  $\{e'_i\}$ , where the process is defined over an infinite number of samples. (Note that the term *quantization error* is defined here as the error due to the operation of the regular (ideal) quantizer, while the error,  $e$ , representing the total error between the actual (nonideal) quantizer input and the quantizer output, and defined by

$$e_i = p_i - q(y_i) \quad (4)$$

is termed the *quantization noise* [8]).

When considering the quantizer output, one of two distinct definitions of signal error will be relevant, these being the deviations from either the perturbed or unperturbed inputs. The appropriate choice depends on whether the sinusoidal perturbation in the system under consideration is predominantly due to the actual rate variation caused by shaft or bearing imbalance, or to sensor nonideality.

When  $v_a$ , the average rate of change of signal  $p$  is irrational, the processes  $\{p\}$  and  $\{y\}$ , generated from the fractional parts of  $p$  and  $y$ , are both uniformly distributed over  $[0, 1)$  when an infinite sample is considered [2], [4]. If the sinusoidal perturbation under investigation is due to encoder nonideality, and

the shaft velocity is constant, the instantaneous rate of change of  $y$  is given by

$$\dot{y}_i = v_a + 2\pi(v_a/L)A \cos(2\pi(v_a/L)i). \quad (5)$$

Conversely, if the sinusoidal variation is present in the shaft rotation,  $p$  and  $y$  become identical, and the rate of change of the input to the ideal quantizer is again given by (5).

The signal error of the quantiser output (from the unperturbed, constant rate input) is the quantization noise

$$\begin{aligned} e &= v_a i - \lfloor y + \frac{1}{2} \rfloor \\ &= v_a i + A \sin(2\pi(v_a/L)i) \\ &\quad + \frac{1}{2} - \lfloor v_a i + A \sin(2\pi(v_a/L)i) + \frac{1}{2} \rfloor \\ &\quad - A \sin(2\pi(v_a/L)i) - \frac{1}{2} \\ &= [\langle v_a i + A \sin(2\pi(v_a/L)i) + \frac{1}{2} \rangle - \frac{1}{2}] \\ &\quad - A \sin(2\pi(v_a/L)i) \\ &= e' - w_s \end{aligned} \quad (6)$$

where  $e'$  is the quantization error of the process  $\{v_a i + A \sin(2\pi(v_a/L)i)\} = \{v_a i + w_s\}$ , and  $w_s$  is the sinusoidal perturbation  $A \sin(2\pi(v_a/L)i)$ .

#### A. Rate Error Spectra of Sinusoidally Perturbed, Nominally Constant Rate Systems

Using (3), the Fourier series expansion of the quantization error,  $e'$ , in the presence of the sinusoidal perturbation, can be written as

$$\begin{aligned} e'_i &= \sum_{k \neq 0} -\frac{1}{2\pi j k} \\ &\quad \cdot \exp[2\pi j k [v_a i + A \sin(2\pi(v_a/L)i)]] \\ &= \sum_{k \neq 0} -\frac{1}{2\pi j k} e^{2\pi j k v_a i} \\ &\quad \cdot \exp[2\pi j k A \sin(2\pi(v_a/L)i)]. \end{aligned} \quad (7)$$

The latter exponential terms can be represented by a summation of Bessel functions using the Jacobi-Anger formula [9]

$$e^{jz \sin \Theta} = \sum_{m=-\infty}^{\infty} J_m(z) e^{j m \Theta}. \quad (8)$$

Hence, (7) can be rewritten as

$$\begin{aligned} e'_i &= \sum_{k \neq 0} -\frac{1}{2\pi j k} e^{2\pi j k v_a i} \sum_{m=-\infty}^{\infty} J_m(2\pi k A) \\ &\quad \cdot \exp[j m (2\pi v_a i / L)] \\ &= \sum_{m \in \mathbb{Z}; k \neq 0} -\frac{1}{2\pi j k} J_m(2\pi k A) \\ &\quad \cdot \exp[2\pi j k v_a [i + (m/L)]]. \end{aligned} \quad (9)$$

Equation (9) expresses the error  $e'$  in the form of a generalized Fourier series [10], indicating that finite Fourier coefficients

exist at all frequencies given by  $f = \langle k v_a [i + (m/L)] \rangle$ ,  $m$  an integer. In the absence of the sinusoidal component, the spectrum of the almost periodic error introduced by the quantizer consists of discrete spectral components at  $f = \langle k v_a i \rangle$ , so that the  $m$  terms are seen to represent the sidebands introduced by the sinusoidal perturbation source. The power spectrum of the quantization error is easily determined by evaluating the magnitudes of the squares of the spectral coefficients, i.e.

$$\begin{aligned} P_{e'}(f) &= \frac{J_m^2(2\pi k A)}{4\pi^2 k^2} \\ &\quad \forall f \text{ s.t. } f = \langle k v_a [i + (m/L)] \rangle \\ &\quad m \in \mathbb{Z}, k \neq 0. \end{aligned} \quad (10)$$

By considering the properties of a simple digital differentiator, the corresponding rate error spectrum is easily obtained as

$$\begin{aligned} P_{v'}(f) &= 2(1 - \cos(2\pi k v_a [i + (m/L)])) P_{e'} \\ &= \frac{J_m^2(2\pi k A)}{2\pi^2 k^2} (1 - \cos(2\pi k v_a [i + (m/L)])) \\ &\quad \forall f \text{ s.t. } f = \langle k v_a [i + (m/L)] \rangle \\ &\quad m \in \mathbb{Z}, k \neq 0. \end{aligned} \quad (11)$$

Examination of (6) illustrates that  $P_e(f)$ , the spectrum of the total signal error,  $e$ , (where the sinusoidal perturbation is assumed to originate from sensor error), is identical to that of  $e'$  except for an additional term (of magnitude  $A^2/4$ ) at frequency  $f = \langle v_a/L \rangle$ . Similarly, the associated rate error,  $P_{v'}(f)$ , is equivalent to that given by (11), with the addition of a component of magnitude  $(A^2/2)(1 - \cos(2\pi v_a/L))$  at  $f = \langle v_a/L \rangle$ . It is noted that this component is very small for low-frequency perturbations (when  $v_a/L \ll 1$ ), due to the slow rate of change of the sinusoidal component under these conditions.

#### B. Numerical Investigation of Spectra of Sinusoidally Perturbed Signals

Because of the potentially large number of significant line intensities, it is useful to consider the number of  $k$  and  $m$  terms of (11) to be included in the computational generation of theoretical spectra. When  $\langle v_a \rangle$  is close to 0 or 1, it is found that the number of  $k$  terms considered,  $k_{\max}$ , should be large (100 or more). Otherwise, a lower value (20-40) will give satisfactory results.

The term  $2\pi k A$  has an equivalence to the modulation index,  $\beta$ , in FM systems. An approximate expression for the bandwidth,  $B$ , of the modulated signal is provided by Carson's rule

$$B \approx 2(\beta + 1)f_m \equiv 2(2\pi k A + 1)\langle v_a/L \rangle \quad (12)$$

where the modulating frequency  $f_m$ , is that of the perturbing signal. Due to the nonsinusoidal carrier, as evidenced by the  $k$  variable in (12), it is seen [e.g., from (11)] that each line intensity component of the original unperturbed error signal is modulated to yield a range of line intensities. Low values of  $A$  and  $k$  lead to narrow-band spectral contributions, while the higher modulation index corresponding to higher values of  $k$  results in more spectral contributions of relatively significant magnitudes.

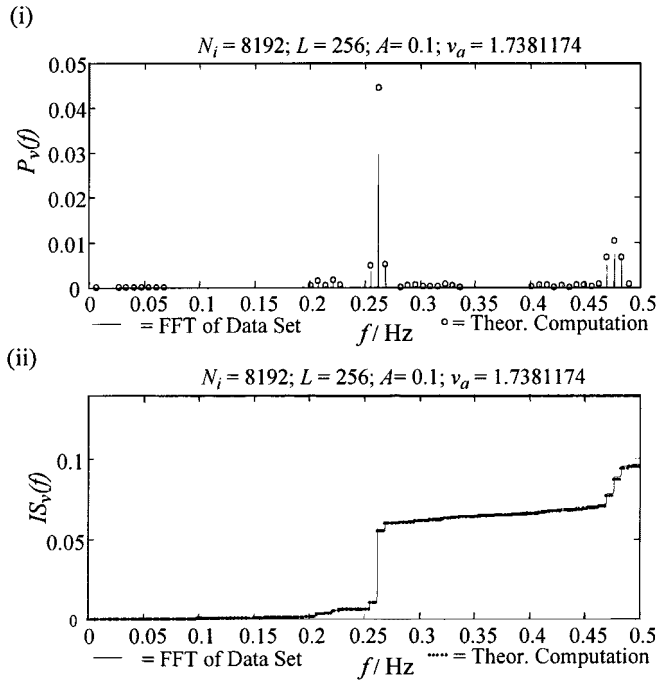


Fig. 2. Spectral plots based on a computer model of a sensor which exhibits a sinusoidal nonideality, when the input rate is constant: (i) Power spectrum,  $P_v(f)$ , with  $k_{\max} = 6$ ; (ii) integrated spectrum,  $IS_v(f)$  with  $k_{\max} = 40$ .

A suitable variant of Carson's rule, given the nonsinusoidal modulating signal and the fact that  $\beta$  takes on noninteger values, is

$$-\lfloor 2\pi kA \rfloor - 2 \leq m \leq \lfloor 2\pi kA \rfloor + 2. \quad (13)$$

Because application of Carson's rule can cause some reasonably significant power components to be disregarded, a slightly wider domain of  $m$  values is usually chosen.

Fig. 2 shows the spectra derived for a finite-length data set, when  $A = 0.1$ ,  $L = 256$ , and  $v_a = 1.73811745$ . For clarity, the power spectrum of the rate error is generated using  $k_{\max} = 6$ , while the integrated spectrum is produced using  $k_{\max} = 40$  to ensure that most significant energy sources are included in the theoretical spectrum. It is seen that the spectral leakage intrinsic to the FFT of the discretely sampled data points leads to erroneous estimates of the discrete spectral peaks when applying this transform. However, use of the integrated spectrum minimizes the visual consequences of this defect and facilitates comparison between the theoretical and experimental spectra. The sidebands introduced by the sinusoidal perturbation are obvious, as is the veracity of the theoretically derived integrated spectrum.

### III. INFLUENCE OF UNIFORMLY DISTRIBUTED NOISE ON SPECTRUM OF PERTURBED CONSTANT RATE SIGNAL

To create a realistic model of a typical physical system, transition noise,  $w$ , (uniformly distributed in  $[-\varepsilon, +\varepsilon]$ ) is added to the low-frequency perturbation, as shown earlier in Fig. 1. The analysis of this system is analogous to that of [2], insofar as the independence of the uniform noise and the quantization error implies that the corresponding characteristic functions can be

multiplied when deriving error measures and spectra. However, the derivation of theoretical spectra is prohibited in this case by the lack of closed-form solutions for some of the resulting expressions. Instead, the assumption is made that: 1) the influence of the uniform noise on the continuous spectral components of a sinusoidally perturbed, constant-rate system is identical to its influence on a similar system which is not subject to the sinusoidal perturbation, and 2) its relative, attenuating effect on the discrete components of the spectrum is identical to that of the case without a sinusoidal perturbation. These assumptions are intuitively reasonable, particularly when the sinusoidal component is small. The rate error spectra of a constant-rate system, with and without transition noise, are

$$S_v(f) = 2[1 - \cos(2\pi f)] \cdot \left[ \varepsilon^2/3 + \frac{1}{12} - \frac{\langle 2\varepsilon \rangle^2}{48\varepsilon^2} [1 - 2\langle 2\varepsilon \rangle + \langle 2\varepsilon \rangle^2] + \sum_{k \neq 0} \frac{1}{4\pi^2 k^2} \frac{\sin^2(2\pi k\varepsilon)}{(2\pi k\varepsilon)^2} \delta(f - \langle kv \rangle) \right] \quad (14)$$

and

$$S_v(f) = 2[1 - \cos(2\pi f)] \left[ \sum_{k \neq 0} \frac{1}{4\pi^2 k^2} \delta(f - \langle kv \rangle) \right] \quad (15)$$

respectively, as derived in [2]. (Use of the Dirac delta function facilitates the accommodation of both discrete line intensity components and a power spectral density function within a single equation). Analogously, when both integral and differential noise are present, the resultant rate error spectrum of the quantization error process  $\{e'\}$ , can be obtained by replacing the  $(1/4\pi^2 k^2)^2$  term of (14) by  $(J_m(2\pi kA)/4\pi^2 k^2)^2$ , where the frequencies of the line intensities are now as given by (11), so that

$$S_{v'}(f) = 2[1 - \cos(2\pi f)] \cdot \left[ \varepsilon^2/3 + \frac{1}{12} - \frac{\langle 2\varepsilon \rangle^2}{48\varepsilon^2} (1 - 2\langle 2\varepsilon \rangle + \langle 2\varepsilon \rangle^2) + \frac{\sin^2(2\pi k\varepsilon) J_m^2(2\pi kA)}{16\pi^4 k^4 \varepsilon^2} \cdot \delta(f - \langle kv_a [i + (m/L)] \rangle) \right], \quad m \in \mathbb{Z}; k \neq 0. \quad (16)$$

The corresponding rate error spectrum of the quantization noise process  $\{e\}$  is

$$S_v(f) = 2[1 - \cos(2\pi f)] \cdot \left[ \varepsilon^2/3 + \frac{1}{12} - \frac{\langle 2\varepsilon \rangle^2}{48\varepsilon^2} (1 - 2\langle 2\varepsilon \rangle + \langle 2\varepsilon \rangle^2) + \frac{\sin^2(2\pi k\varepsilon) J_m^2(2\pi kA)}{16\pi^4 k^4 \varepsilon^2} \delta(f - \langle kv_a [i + (m/L)] \rangle) + \frac{A^2}{4} \delta(f - \langle v_a/L \rangle) \right], \quad m \in \mathbb{Z}; k \neq 0 \quad (17)$$

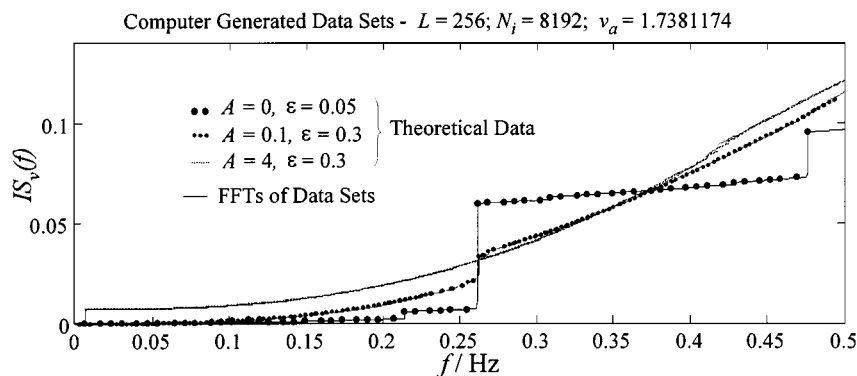


Fig. 3. Integrated spectral plots based on computer models of different sensors which exhibit both sinusoidal nonlinearities and uniformly distributed noise, at a particular input rate,  $v_a$ .

and the theoretical integrated spectrum is

$$\begin{aligned}
 IS_v(f) = & \left[ 2f - \frac{1}{\pi} \sin(2\pi f) \right] \\
 & \cdot \left[ \varepsilon^2/3 + \frac{1}{12} - \frac{\langle 2\varepsilon \rangle^2}{48\varepsilon^2} (1 - 2\langle 2\varepsilon \rangle + \langle 2\varepsilon \rangle^2) \right] \\
 & + \sum_{f' \in [0, f]} 2[1 - \cos(2\pi f')] \\
 & \cdot \left[ \frac{\sin^2(2\pi k\varepsilon) J_m^2(2\pi kA)}{16\pi^4 k^4 \varepsilon^2} + \frac{A^2}{4} \cdot (f \leq \langle v_a/L \rangle) \right]
 \end{aligned} \quad (18)$$

where the summation is of all line intensity terms for which  $f' \leq \langle kv_a[i + (m/L)] \rangle$ . The last term includes a logical switch, so that it is included when the frequency of the sinusoidal perturbation is within the  $[0, f]$  domain.

#### A. Numerical Verification of the Spectral Formulae with Sinusoidal and Uniformly Distributed Noise

Computer-generated, finite-length data sets, including both a low-frequency sinusoidal disturbance and uniformly distributed transition noise, are used to verify the spectral formulae of the previous section. Integrated spectra of data sets for signals with added sinusoidal components of differing magnitudes, as well as differing amounts of added transition noise, are compared in Fig. 3. The theoretical predictions of the spectra match very closely with the spectra obtained using the computed-generated data sets. The theoretical integrated spectrum obtained when  $A = 4$  and  $\varepsilon = 0.3$  exhibits a large number of significant line intensity components, as discussed above. In this case, the largest spectral component is that due to the fundamental of the sinusoidal perturbation. This manifests itself as a step in the integrated spectrum at a low frequency (equal to  $v_a/L$ ), the largest single frequency component of the rate error. As with the other spectra shown, it is clear that the theoretically derived spectra provide a very accurate match to those derived experimentally. A comprehensive series of tests showed that the approximations adopted in the derivation of the theoretical spectra were justified for a wide range of noise-affected systems, including all those which would be encountered in real sensors.

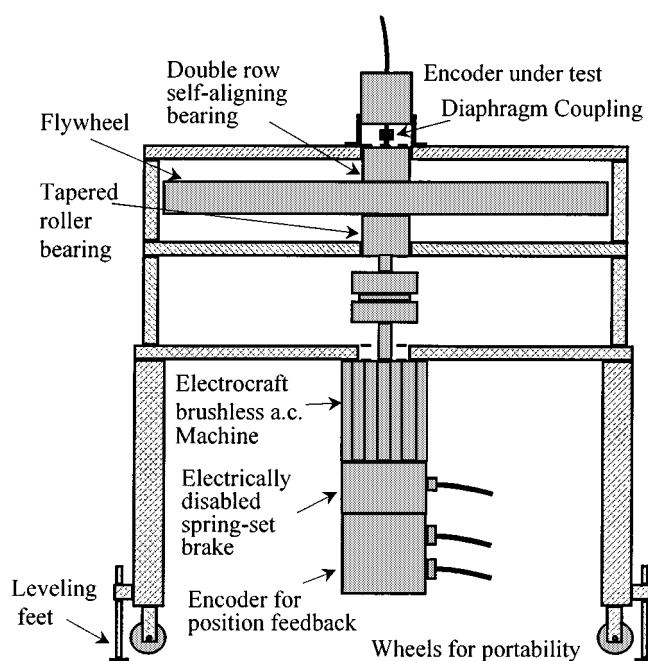


Fig. 4. Custom-designed rig used in the analysis of encoder characteristics.

#### IV. EXPERIMENTAL RESULTS FOR A PULSE COUNT, DIGITAL TACHOMETER USING AN OPTICAL ENCODER SENSOR

An experimental test-rig for encoder characterization, incorporating a high-inertia flywheel (approximately  $2.0 \text{ kg m}^2$ ), as shown in Fig. 4, was utilized to minimize the influence of undesired shaft speed variation on the experimental results. The servodrive is operated in velocity-loop mode, but is detuned to reduce the possibility of significant frequency components being introduced from this source.

The quadrature output channels from commercially available optical incremental encoders, rotating at nominally constant velocity, were decoded in the normal manner, and data sets corresponding to the digitally differentiated output analyzed to ascertain their error characteristics. The encoder employed in the test from which the spectra shown in Fig. 5 were produced has 5000 tracks per revolution, and in-built interpolation increases its output resolution to 25 000 cycles per revolution per track.

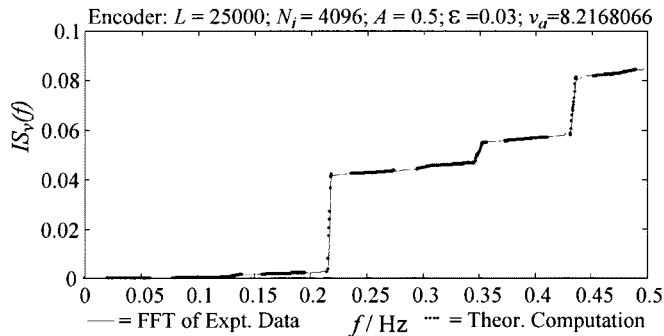


Fig. 5. Integrated spectra (at an arbitrarily chosen shaft speed) derived from experimental output of the encoder-under-test, with prediction by a model using  $\varepsilon = 0.03$  and  $A = 0.5$ .

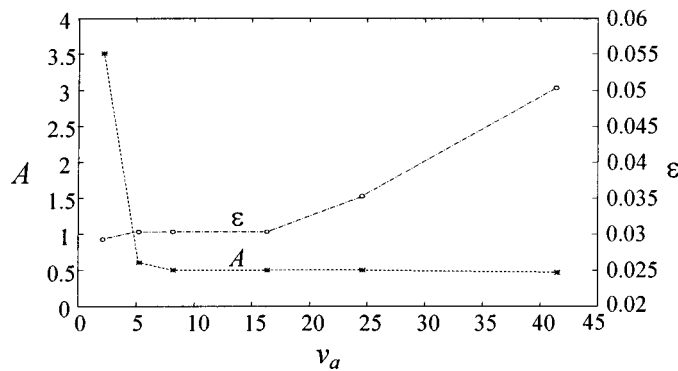


Fig. 6. Model parameters  $A$  and  $\varepsilon$  derived at various encoder shaft velocities, by spectral comparison of the experimental and theoretical integrated spectrum plots generated using the encoder-under-test.

Fig. 5 illustrates that a suitable choice of parameters can produce an excellent match between the spectral characteristic predicted by the theoretical formulae derived above and that generated by performing an FFT on experimental data.

Curve fitting of the theoretical spectra to the experimental FFT-based spectra, through choice of the  $A$  and  $\varepsilon$  model parameters, was performed manually, as this was found to be a relatively quick and straightforward procedure. The pertinent features of the integrated spectrum (magnitude and slope of near-vertical segments in the region of principal spectral components, the presence of sidebands around such components, and the more gradual slope of the integrated spectrum at other frequencies due to differential noise) are used to recursively set both  $A$  and  $\varepsilon$  to achieve good matching.

The model parameters estimated at different rates are plotted in Fig. 6. At low speeds, it is inevitable that the speed of the inertial object under investigation will vary as it rotates, thereby increasing the perceived low-frequency perturbation. At higher speeds, the plot of  $A$  against  $v_a$  is seen to level off. This provides a good justification for the assumption that the dominant low-frequency effect is then due to sensor characteristics, rather than to relative speed variation, which will decrease as speed increases. At high speeds, any temporal dithering (introduced by the slight variations in sampling instants, the finite slew rates of digital signals, the finite temporal resolution of the clocks used in the hardware, etc.), becomes significant and acts to increase

the apparent high-frequency transition noise component. Neither of these effects should be serious at moderate speeds, given a suitable experimental set-up, thereby enabling the determination of a reliable sensor model. Model parameters of approximately  $A = 0.5$  and  $\varepsilon = 0.03$  are seen to be suitable at medium velocities, and can be assumed to represent accurately the sensor itself.

Experiments comparing experimental and theoretical spectra were performed on a number of optical encoders, at a variety of shaft velocities. Good matching was achievable in most cases through correct choices of model parameters. The only notable exception related to a quadrature decoded sensor with significant duty-cycle variation between transitions, because the model does not account for this nonideality. However, a reasonable model for the sensor, with a value of transition noise which is effectively averaged over all encoder edges, is still readily obtainable in this case.

## V. CONCLUSIONS

The effect of manufacturing nonidealities on the output of an incremental encoder has been analyzed in this paper, particularly in the context of the use of digital differentiation for the estimation of shaft velocity. Typical nonidealities are shown to be well modeled by the postulation of two distinct error sources: a uniformly distributed transition noise error and a sinusoidal variation over the circumference of the codewheel. A low-frequency speed variation (at the fundamental frequency of the rotating system) can also be modeled by the latter approximation. Equations for the prediction of the spectral characteristics of this quantity in the presence of the noise sources have been derived, and their veracity demonstrated using both computer-generated and experimentally obtained data.

The results presented were obtained by a recursive, manual curve-fitting procedure. It is found that very good matching can be achieved by a skilled operator within a few minutes. The design of an automated system of optimum parameter estimation through software-based curve-fitting is an interesting task, as the various pertinent features of the integrated spectrum described in Section IV should each be considered, as opposed to performing a simple error minimization over the complete frequency range. Work on this optimization problem is on-going.

The theoretical analysis of the errors inherent in encoder outputs which was presented in this paper, along with that presented previously in [2], provides a comprehensive analytical framework for the investigation of such sensors, or other sources of quantized data, in measurement systems and data converters.

## ACKNOWLEDGMENT

The author wishes to thank the anonymous reviewers for their helpful comments.

## REFERENCES

- [1] C. Yien, "Incremental encoder errors: Causes and ways to reduce them," in *Proc. Int. Incremental Motion Conf. (PCIM'92)*, Nürnberg, Germany, Apr. 1992, pp. 110–121.
- [2] R. C. Kavanagh and J. M. D. Murphy, "The effects of quantization noise and sensor nonideality on digital-differentiator-based velocity measurement," *IEEE Trans. Instrum. Meas.*, vol. 47, pp. 1457–1463, Dec. 1998.

- [3] A. G. Clavier, P. F. Panter, and D. D. Grieg, "Distortion in a pulse code modulation system," *Amer. Inst. Elect. Eng. Trans.*, vol. 66, pp. 989–1005, 1947.
- [4] R. M. Gray, "Quantization noise spectra," *IEEE Trans. Inform. Theory*, vol. 36, pp. 1220–1244, Nov. 1990.
- [5] R. E. Ziemer and W. H. Tranter, *Principles of Communications—Systems, Modulation, and Noise*, 4th ed. New York: Wiley, 1995.
- [6] P. Z. Peebles, Jr., *Communication System Principles*. Reading, MA: Addison-Wesley, 1976.
- [7] M. W. Schwartz, W. R. Bennett, and S. Stein, *Communication Systems and Techniques*. New York: McGraw-Hill, 1966.
- [8] R. M. Gray and T. G. Stockham, Jr., "Dithered quantizers," *IEEE Trans. Inform. Theory*, vol. 39, pp. 805–812, May 1993.
- [9] N. W. McLachlan, *Bessel Functions for Engineers*. Oxford, U.K.: Oxford Univ. Press, 1934, (Revised printing: 1941).
- [10] E. Kreyszig, *Advanced Engineering Mathematics*, 4th ed. New York: Wiley, 1979.



**Richard C. Kavanagh** (M'95) was born in Cork, Ireland, in 1961. He received the B.E., M.Eng.Sc., and Ph.D. degrees in electrical engineering from the National University of Ireland in 1984, 1985, and 1998, respectively.

He is a College Lecturer with the National University of Ireland, where he directs the Mechatronics Research Laboratory. He has previously worked as a Senior Research Scientist with PEI Technologies, University College, Cork, to whom he is currently a Consultant. He has also worked as a Senior Project Engineer with SPS Laboratories Ltd. His present research interests include improved sensor design, the analysis of quantization effects in data acquisition systems, hardware-in-the-loop test systems, and the design of advanced intra-machine communications systems.